Poly(vinylidene fluoride) porous membranes precipitated in water/ethanol dual-coagulation bath: The relationship between morphology and performance in vanadium flow battery

Jingyu Cao [a,b], Huamin Zhang [a,*], Wanxing Xu [a,b], Xianfeng Li [a,*]

[a] Division of Energy Storage, Dalian Institute of Chemical Physics, Chinese Academy of Sciences, Dalian 116023, PR China
[b] University of Chinese Academy of Sciences, Beijing 100039, PR China

HIGHLIGHTS

- PVDF porous membranes with tunable morphology are prepared for VFB application.
- The membrane morphology is facilely tuned via water/ethanol coagulation bath.
- The membrane performance in VFB can be optimized via morphology control.
- The PVDF membrane indicates a prospective candidate for VFB separator.

ARTICLE INFO

ABSTRACT

Poly(vinylidene fluoride) (PVDF) porous membranes with tunable morphology are facilely prepared via dual-coagulation bath by phase inversion method and investigated in vanadium flow battery (VFB). Water/ethanol solutions with different compositions are selected as the coagulation baths and the effect of water/ethanol including content ratio and immersion time on membrane morphology is studied in detail. SEM results indicate the increased degree of crystallization and surface roughness of prepared membranes with higher ethanol content in coagulation bath and longer immersion time. In addition, β phase is a dominated crystalline form in these membranes. The upper surface pore size variety and overall crystalline structure lead to a non-monotonous change of ions permeability and area resistance. As a result, the coulombic efficiency decreases on the whole with volume ratio of water/ethanol ranging from 10:0 to 3:7, whereas there is a raised peak at the ratio of 5:5. Meanwhile, the voltage efficiency of these membranes exhibits an opposite tendency. Therefore, the morphology and property of PVDF porous membranes can be adjusted via changing the composition of coagulation bath. This research presents an effective and feasible method to optimize the fabrication parameters of PVDF porous membranes for VFB application.

1. Introduction

The increasing interest in renewable energy can be partially attributed to the issues of environmental pollution and serious energy scarcity brought by excessively use of fossil fuels. To overcome the shortage of random and intermittent renewable resources, energy storage is necessarily combined to offer a well-established approach for improving the grid reliability and utilization [1]. Among the energy storage techniques, vanadium flow battery (VFB) represents an excellent candidate for the integration of renewable resources due to its advantages like independent design of output power and energy storage capacity, long cycle life as well as high safety [2,3].

A VFB single cell consists of two electrolyte flow compartments separated by an ion-selective membrane. The membrane is employed to separate the positive and negative electrolyte as well as complete the internal current circuit by transferring cations or anions. An ideal ion exchange membrane (IEM) should possess good ion conductivity, high ion selectivity as well as excellent chemical stability [4]. Several types of membranes are investigated for VFB application, including perfluorosulfonic membranes, non fluorinated membranes and porous nanofiltration (NF) membranes. Perfluorosulfonic membranes, such as DuPont's Nafion®, are widely used in VFB due to their high conductivity and chemical

* Corresponding authors. Tel.: +86 411 84379669; fax: +86 411 84665057.
E-mail addresses: zhanghm@dicp.ac.cn (H. Zhang), lixianfeng@dicp.ac.cn (X. Li).

stability. However, the extremely high cost and relatively low ion selectivity hinder their commercialization in VFB [5]. Non fluorinated polymer membranes like aromatic poly cations and poly anions show remarkable efficiency in VFB. However, they are prone to decompose especially in strong acid and oxidation environment due to the introduction of ion exchange groups [6,7].

Recently, porous nanofiltration (NF) membrane separators were successfully applied in VFB based on the idea of tuning V/H selectivity via pore size exclusion, charge density, etc [8]. Several kinds of porous membranes were fabricated and investigated in VFB application, among which poly(vinylidene fluoride) membranes showed an impressive stability (kept stable after running more than 1000 cycles) and performance [9].

Actually, PVDF membranes have been extensively applied in water treatment, membrane distillation due to their outstanding mechanical stability and chemical resistance to aggressive reagents, yet have the advantage of simple production and low cost [10]. As a semi-crystalline polymer, it possesses at least four distinct phases, known as α, β, γ and δ [11]. The phase separation process, which is normally adapted for membrane fabrication, is controlled by liquid–liquid demixing or liquid–solid demixing (crystallization) during immersion precipitation [10]. Generally, polymer crystallization and the resultant membrane morphology precipitated in coagulation bath are the most important factors in determining the ultimate performance. These properties are affected by a variety of experimental parameters like the temperature and composition of polymer solution (polymer, solvent, additives and their respective concentrations) [12–14], the temperature and components of coagulation bath medium [15], the resolving temperature [16], the evaporation time [13], the membrane thickness [17], the ambient humidity as well as the type of support material.

In the present research, investigation was undertaken to study the effect of coagulation medium on the PVDF membrane morphology and further on their performances. The morphology and properties of prepared membranes were investigated in detail, indicating a simple and effective way of membrane morphology control. Moreover, attempts have been made to correlate the morphology and membrane performance in VFBs, thus to provide a potential approach of fabricating high performance VFB membranes.

2. Experimental

2.1. Membrane preparation

The PVDF (Shanghai 3F New Materials Company Ltd, FR904) was dissolved in DMAC to form 23 wt% of solutions. The solution was cast onto a glass plate with thickness of 155 ± 5 μm. The plate was first immersed in water/alcohol bath for a certain time and then passed through water bath to complete solidification process. The composition and immersion time of mixed bath were adjusted to tune membrane morphology. The detailed information of resulted membranes precipitated in different coagulation bath was shown in Table 1.

2.2. Membrane characterization

2.2.1. Scanning electronic microscopy (SEM)

The cross-section and surface morphology of the membrane were observed by SEM. The samples were fractured in liquid nitrogen and then were coated with gold before SEM analysis.

2.2.2. Water contact angle

The water contact angle was measured by the sessile drop method (JC2001A, POWER-EACH®, Shanghai Zhongchen Digital Technic Apparatus Co. Ltd., China). 3 μl deionized water was

Table 1
Physicochemical properties of prepared PVDF membranes.

Membrane	Volume ratio (water/EtOH)	Time[a]	Contact angle	Area resistance (Ω cm^2)	Porosity (%)
M1	10:0	1 min	85.0°	2.14	47.2
M2	9:1	1 min	85.5°	1.47	47.8
M3	7:3	1 min	83.0°	1.45	46.1
M4	5:5	1 min	73.5°	2.61	43.9
M5	3:7	1 min	75.0°	0.81	51.0
M6	0:10	1 min	73.0°	0.30	53.7
M7	5:5	3 min	–	1.50	–
M8	5:5	7 min	–	1.11	–

[a] The time is referred to the immersion time in water/ethanol coagulation bath.

dropped onto flat membrane surface and the image was frozen after 5 s for each test.

2.2.3. Crystalline phase

Identification of the crystalline phase of PVDF membranes was carried out by using X-ray diffractograms (XRD) and Fourier Transform Infrared Spectroscopy (FTIR). XRD was carried out by positioning the PVDF membrane on glass slide mounted on an SX-2700 diffractometer using Cu Kα radiation. Intensities were recorded in the range $10° < 2\theta < 35°$, typically with sweeping rate $0.01°$ s^{-1}. FTIR spectra of membrane were detected by JASCO FTIR 4100 spectrometer over a frequency range of 4000–600 cm^{-1}.

2.2.4. Porosity

The suitable cut PVDF membranes were immersed in deionized water to be fully saturated. The wet membranes were weighed after wiping up the surface water with filter paper. Then the samples were dried in vacuum oven at 85 °C for 24 h and weighed. The membrane porosity is calculated by Eq. (1):

$$\varepsilon = \frac{\left(m_{\text{wet}} - m_{\text{dry}}\right)/\rho}{s \times d} \times 100\% \quad (1)$$

Where ε is the porosity of the membrane, m_{wet} and m_{dry} are the mass of wet membrane and dry membrane respectively, ρ is water density, s is membrane area, d is membrane thickness.

2.2.5. Pure water flux

Pure water flux was done in a stainless steel dead-end pressure cell with effective membrane area of 19.6 cm^2. After the water was poured in the cell, the device was pressurized with nitrogen and then kept at 3.6 MP. Permeate samples were collected in cooled flasks as a function of time, weighed and analyzed.

The permeation was stopped when the membrane flux reached a constant value. All the measurements were based on at least three samples and the average values were used. The standard deviation on the measurements is about 5%. The water permeating flux is calculated by Eq. (2):

$$J = \frac{m}{\rho \times s \times t} \quad (2)$$

Where J is pure water flux, m and ρ are the water mass and water density respectively, s is the effective area of tested membrane, t is the water permeation time of each sample.

2.2.6. Vanadium permeability

The permeability of VO^{2+} ions was detected in diffusion cell with the membrane in between [18]. The left cell was filled with 1.5 M VOSO$_4$ in 3 M H$_2$SO$_4$ solution, while the right one is filled with 1.5 M MgSO$_4$ in 3 M H$_2$SO$_4$ solution to equalize the ionic strength

and minimize the osmotic pressure effect. The volume of each cell was 76 mL and the effective membrane area was 9 cm^2. Magnetic stirrer was used at both sides to avoid polarization. Samples from the right cell were collected at regular time intervals and to be detected by automatic potentiometric titration. The VO^{2+} permeability was calculated according to the Ficker diffusion law shown as Eq. (3):

$$V_B \frac{dC_B(t)}{dt} = A \frac{P}{L}(C_A - C_B(t)) \tag{3}$$

Where V_B is the solution volume in the right reservoir, A and L are the effective area and thickness of the membrane, respectively. P is the permeability of the VO^{2+} ions. C_A is the ion concentration in the left reservoir. $C_B(t)$ is the ion concentration in the right reservoir as a function of time.

2.2.7. Area resistance

Membrane area resistance was detected with a conductivity cell containing 0.5 mol H$_2$SO$_4$ in each chamber, which was separated by a membrane with 1 cm^2 active area [19]. Electrochemical impedance spectroscopy (EIS) was utilized to determine r_1 and r_2. The area resistance r was obtained by Eq. (4):

$$r = (r_1 - r_2) \times S \tag{4}$$

Where r_1, r_2 indicates the cell resistance with and without a membrane respectively, S is the effective area.

2.2.8. Single cell performance

The VFB single cell was fabricated by sandwiching a membrane between two carbon felt electrodes, clamped by two graphite polar plates. All these components were fixed by two stainless plates. In the cell system, 30 mL of 1.5 M V^{2+}/V^{3+} in 3 M H$_2$SO$_4$ and of 1.5 M VO^{2+}/VO^{2+} in 3 M H$_2$SO$_4$ solution serving as electrolytes at the negative and positive sides respectively were pumped through each electrode. The charge and discharge test was carried out by an Arbin BT2000 with different current densities. The cut-off voltage for the charge and discharge process was set between 1.65 V and 0.8 V.

3. Results and discussion

3.1. Morphology

The cross-section of PVDF membranes precipitated from different dual-coagulation bath was observed by SEM and demonstrated in Fig. 1(a)–(d). As the ratio of ethanol in coagulation bath raises, the membrane morphology changes from asymmetric structure with finger-like voids to symmetric structure with spherical particles, accompanying diminishing macrovoids. The results in Fig. 1(a) depicts a typical instantaneous liquid−liquid demixing structure consisting of a dense surface, a voids sublayer and a sponge-like middle zone, formed in pure water bath, whereas the membrane precipitated from ethanol (Fig. 1(d)) exhibits a much thicker interconnected structure, known to be derived from delayed demixing.

As a semi-crystalline polymer, the phase separation process of PVDF is more complicated than amorphous polymers, governing by liquid−liquid demixing and liquid−solid demixing (crystallization) mechanisms [10]. Coagulation medium is a key factor in determining the dominate mechanism during phase separation. When ethanol is added into water coagulation during immersion precipitation, gelatin boundary in ternary phase diagrams is further away from the PVDF−DMAc axis, which indicates stability enhancement of EtOH/DMAc/PVDF system [20]. The phenomenon is attributed to smaller solubility parameter difference between ethanol ($\delta_{t,\ E-D}$) and DMAc than that between water and DMAc ($\delta_{t,\ W-D}$). In other words, the mutual affinity and compatibility between ethanol and DMAc increases, thus more non-solvent is needed to precipitate from coagulation bath, resulting in a delayed demixing process.

Furthermore, ethanol in water bath also causes kinetic hindrance due to changed diffusion coefficient (D) between non-solvent and solvent, which is regarded as a qualitative prediction of mass exchange rate. It is reported that $D_{DMAc-in-EtOH}$ is similar with $D_{DMAc-in-water}$, while $D_{EtOH-in-DMAc}$ is 40 times lower than $D_{water-in-DMAc}$ [21]. As a result, the precipitation rate decreases with a decline in diffusion coefficient when solidified in ethanol. Obviously, thermodynamic property and the kinetic nature have a coincident influence on membrane forming process and finally induce more crystallization due to prolonged demixing process. In addition, membrane precipitated in pure ethanol (Fig. 1(d)) is rather thick due to hampered exchange rate and ethanol swelling [15,22].

Besides, the effect of immersed time in water/ethanol bath on membrane morphology was investigated as well (Fig. 2(a)−(c)). M4, M7 and M8 were fabricated in 5:5 water/ethanol bath with immersion time of 1 min, 3 min and 7 min, respectively. The cross-section becomes much more symmetric with increasing crystallization degree and more perfect spherical partials were formed in consequence of liquid−solid demixing. For example, M8 with immersion time of 7 min shows a totally symmetric, compressed cross-section with much smaller particles compared with M4 with immersion time of 1 min.
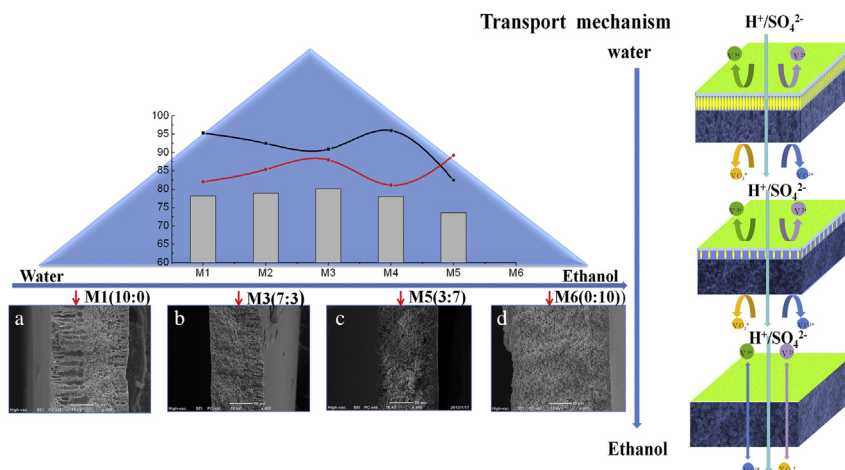

Fig. 1. Cross-section morphology of PVDF membranes with respect to its performance in VFB and membrane transport mechanism (a. M1 b. M3 c. M5 d. M6).
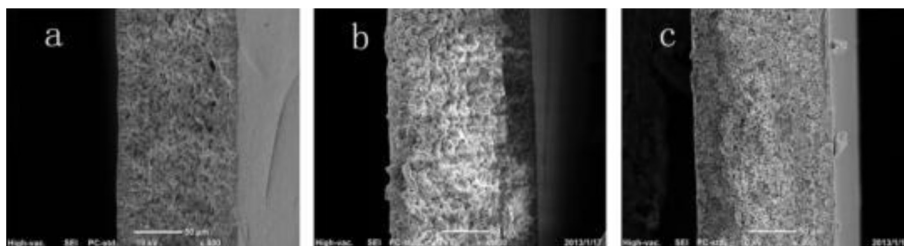
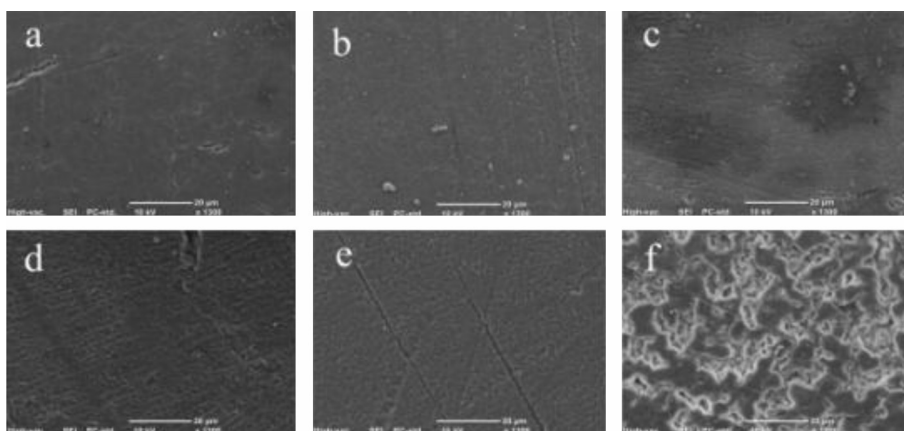**Fig. 2.** Cross-section morphology of PVDF membranes (a. M4 b. M7 c. M8).

Fig. 3. Surface morphology of PVDF membranes (a. M1 b. M2 c. M3 d. M4 e. M5 f. M6).

In addition, the upper surface morphology was shown in Fig. 3(a)–(f). It is obviously that with more ethanol in non-solvent, the surface roughness of membrane increases. For example, the surface of M1 is so smooth that concave–convex can be barely observed, while M5 exhibits a much uneven appearance.

3.2. Crystalline phases

Normally four crystalline phases, designed as α (Form II), β (Form I), γ (Form III) and δ (Form II′) are existed in PVDF. The different phases can be distinguished by the conformation of the C–C bonds along the backbone. For example, β-form has an s-trans conformation (TTTT) while α-form has an alternating s-trans and s-gauche bonds (TGT$\overline{G}$). Generally, FTIR combined with XRD can be used to identify the crystalline phases of PVDF. As shown in Fig. 4, β characteristic peaks at 840 and 1275 cm^{-1} can be observed in FTIR for M1 prepared from pure water whereas the typical α phase peaks at 760 cm^{-1} are visibly sharp in the spectrum of M6 immersed in pure ethanol for 1 min. In addition, peaks at 1275 cm^{-1} become less intensive form M1 to M6, indicating a little decline of β phase crystallization with increasing content of ethanol. The results are verified by means of XRD (Fig. 5) as well. M1 to M5 exhibit similar crystalline reflections at 20.4 ± 0.1°, referred to as diffraction in plane (110) to (200) of the β phase crystal. However, the apparent peaks at 18.4° and 26.6° in M6, which are attributed to α phase, confirming again the formation of more perfect, α phase crystals [15,23]. Thus, it can be concluded that α phase is easier to be prepared in ethanol coagulation bath than that in water bath. However, the intensities of these peaks show an evident prevalence of β phase. The transition is somehow confusing due to delayed demixing favors the formation of β phase, a less stable configuration [15]. To explain this change, polarity of various coagulation baths may be taken into consideration. It is plausible that ethanol with
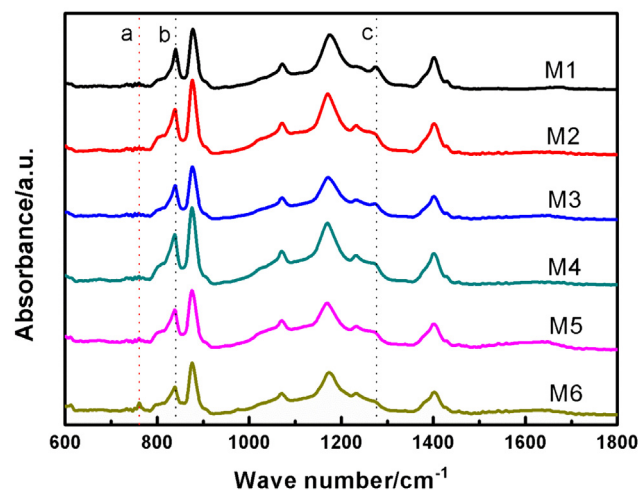

Fig. 4. FTIR spectra of PVDF membranes precipitated in different water/ethanol bath (a. 760 cm^{-1} b. 840 cm^{-1} c. 1275 cm^{-1}).

lower polarity in coagulation bath produces more non-polar α form. Similar phenomenon was observed when polar polymer was added into cast solution inducing polar β phase [24,25]. Moreover, the XRD spectra of M7 and M8 are also shown in Fig. 6. The diminishing peak of α phase indicates a less α crystalline phase formation, which is ascribed to the delayed demixing with prolonged immersion in water/ethanol coagulation, leading to the oriented packing of CH$_2$–CF$_2$ dipoles to form β phase crystals. To conclude, the phase transmission of PVDF membranes is dominated by its medium polarity (including coagulation bath and cast solution) as well as mass transfer rate in membrane precipitation process.
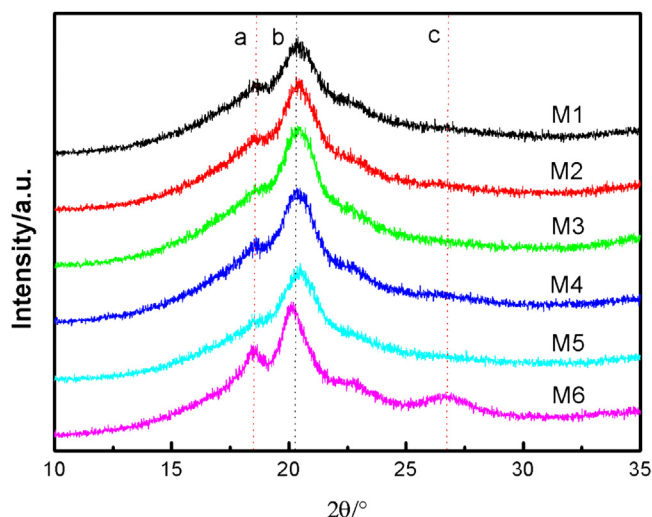
Fig. 5. XRD of PVDF membranes precipitated in different water/ethanol bath (a. 18.4° b. 20.4° c. 26.6°).

Fig. 7. Water flux and vanadium ions permeability of PVDF membranes.

3.3. Hydrophilicity

Table 1 summarized the water contact angles for the upper surface of PVDF membranes, which were prepared from various coagulation baths. The contact angle shows an overall decreasing tendency as the ratio of ethanol increasing. For example, the contact angle of M3 is 83° while that of M4 declines to 73.5°, indicating an enhancement of surface hydrophilicity. The sharp decrease of contact angle can be ascribed to ununiform or rougher surface. Thus, it can be concluded that rougher surface can be formed by using ethanol as non-solvent and the hydrophilic nature can be improved accordingly [26,27].

3.4. Pure water flux (PWF)

PWF was carried out to quantity the mean pore size of prepared membranes. To further link mean pore size with membrane permeability, PWF of prepared membranes was measured at
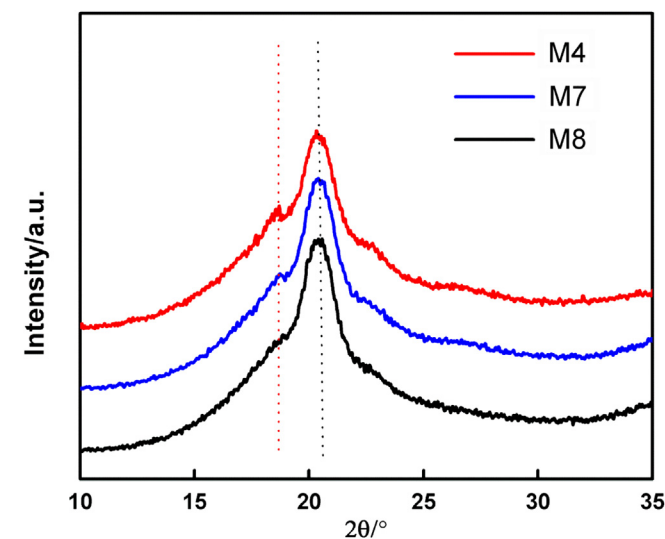

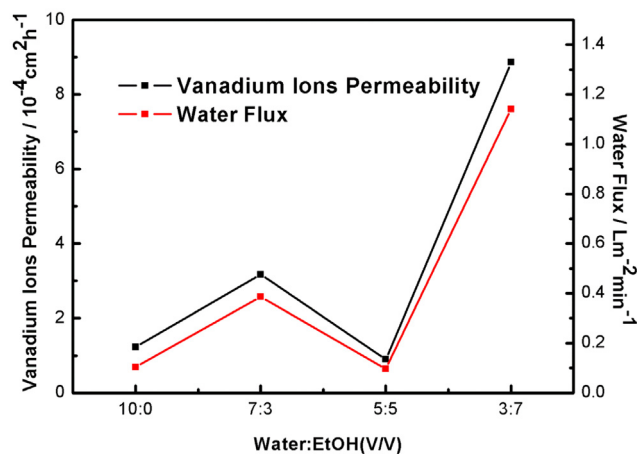**Fig. 6.** XRD of PVDF membranes precipitated in 5:5 water/ethanol bath with different immersion time.

certain pressure and summarized in Fig. 7. The PWF, a criterion of mean pore size, presents a non-monotonic change, i.e., the PWF shows first increasing then decreasing tendency as the ratio of water/ethanol decreasing from 10/0 (M1) to 5/5 (M4), whereas reached the highest PWF at the ratio of 3/7 (M5). Hence, effective pore size can be considered to exhibit the same change trend with higher ethanol ratio in coagulation bath. It was reported that larger mean pore size and wider distribution was observed as the ethanol concentration rising [21,26]. However, PWF of M4 was relatively low in this study. It can be attributed to the co-effect of upper surface pore size variation and compacted bulk zone, which amplifies mass transfer resistance and even blocks some open-end pores. In other words, the over-all structure connectivity changes due to the presence of compressed crystalline partials. Upper surface as well as bulk zone acts as transport barrier, resulting a non-monotonic change in water flux.

3.5. Membrane porosity

The membrane morphology was facially tuned with different coagulation baths, thus resulting varying porosity. It can be seen in Table 1 that the porosity has minor changes from M1 to M3 and shows an overall decreasing tendency from M1 to M4. Further increasing the content of ethanol in coagulation baths, the membrane porosity increases dramatically from M4 to M6. Similar trend has been observed in previous work, i.e., firstly decrease then increase [26]. This change is due to the combined effects of macrovoids diminishing and pore size distribution variety.

3.6. Vanadium permeability

The permeation of vanadium ions with different valance states through the membrane occurs spontaneously and simultaneously, which causes self-discharge and capacity loss. It was reported that the diffusion coefficients of vanadium ions cross Nafion115 are in the order of $V^{2+} > VO^{2+} > VO_2^+ > V^{3+}$ [28]. Given V^{2+} is too active in air to be measured, VO^{2+} ion permeability are detected to couple membrane morphology and selectivity as demonstrated in Figs. 8 and 7. The permeability presents the same tendency compared with that of PWF, which increases firstly then decreases and finally increases. The phenomenon is reasonable since the ion permeability as well as selectivity of membranes is closely related to their pore size distribution.
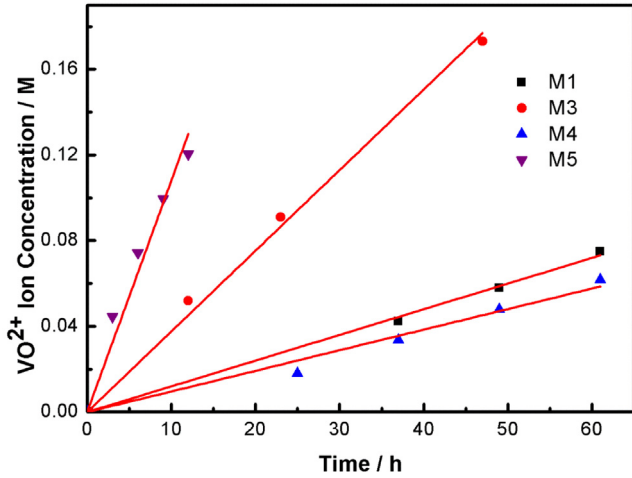
Fig. 8. VO^{2+} concentration in the deficiency side of the permeation measuring device.

3.7. Area resistance

The area resistance of a membrane under VFB circumstances indicates the ion conductivity of membranes, which will finally determine the internal resistance of battery. The area resistance is listed in Table 1, which shows the opposite trend with pure water flux. It is reasonable since the larger pore size membrane with better ion conductivity has lower area resistance for porous membranes. Additionally, the pore size of the skinless M6 is too large to retain protons and vanadium ions therefore all species can go through the interconnected channels freely.

3.8. Single cell performance and life cycle

The VFB single cell performance is demonstrated in Fig. 9. M6 prepared from pure ethanol bath is futile for VFB due to its too large pores. With the proportion of ethanol increasing, the coulombic efficiency (CE), which is defined as the ratio of discharge capacity divided by corresponding charge capacity, decreases on the whole, with volume ratio of water/ethanol ranging from 10:0 to 3:7, whereas there is a raised peak at the ratio of 5:5. Meanwhile,
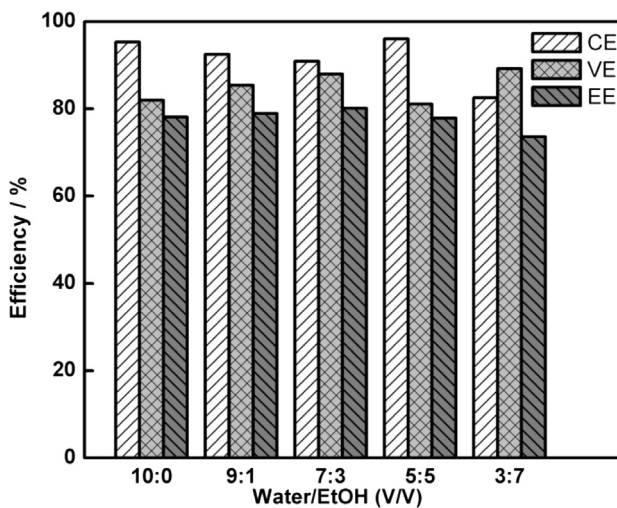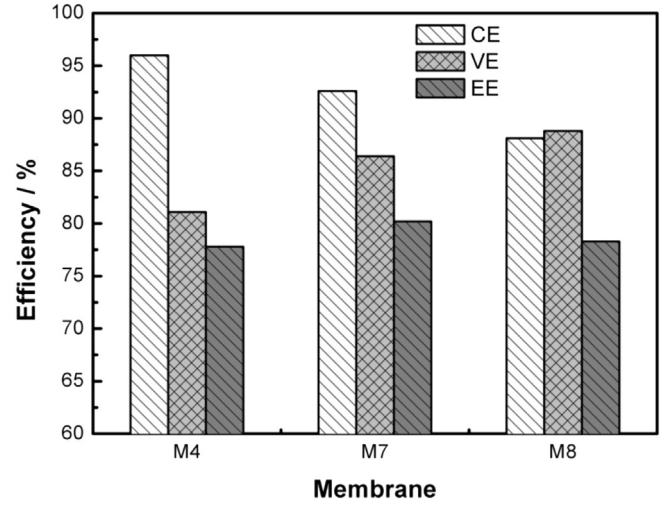

Fig. 10. VFB single cell performance of membranes with different immersion time in water/ethanol coagulation bath (M4.1 min M7.3 min M8.7 min).
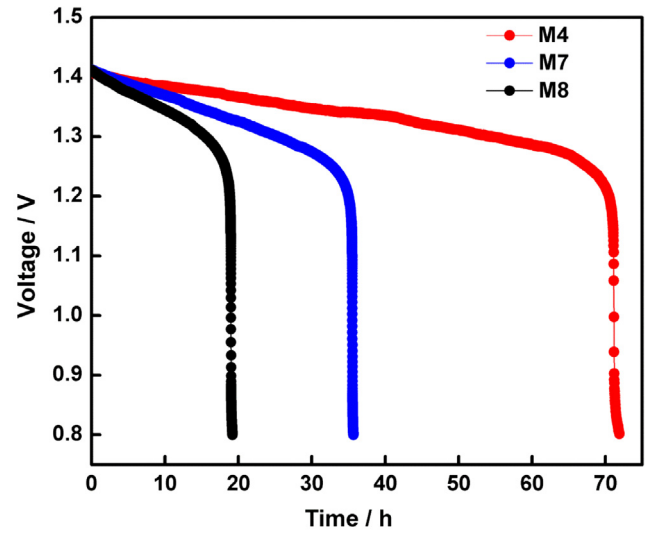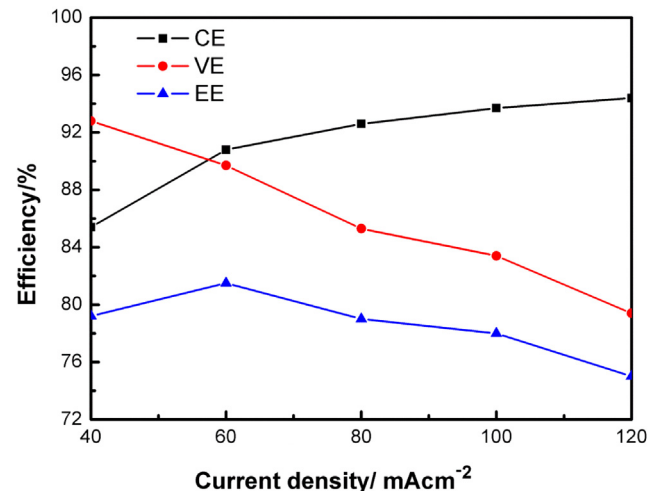

Fig. 11. VFB self-discharge curves.

Fig. 9. VFB single cell performance of membranes precipitated in different water/ethanol coagulation baths.

Fig. 12. VFB single cell performance of M7 under different current densities.
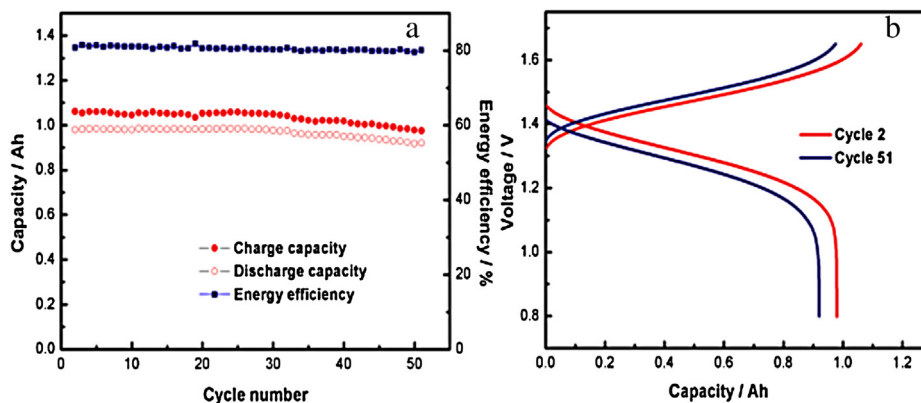
Fig. 13. Performance of VFB single cell with M7: (a) charge–discharge capacity and energy efficiency in 50 cycles; (b) cell–voltage profile with respect to cell capacity in cycle 2 and cycle 51.
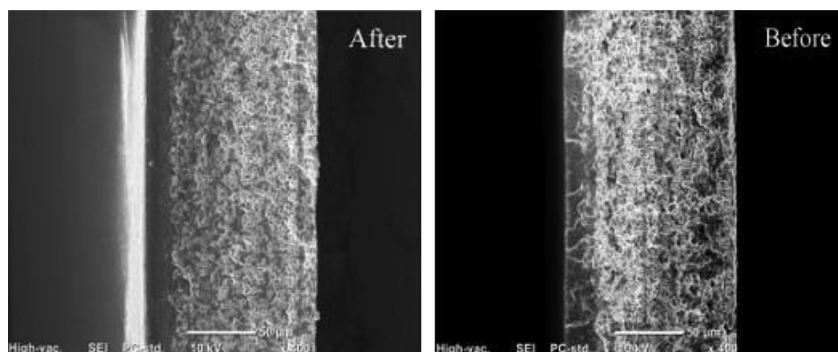

Fig. 14. Membrane morphology before and after running for more than 200 cycles.

voltage efficiency (VE) which is defined as the ratio of mean discharge voltage divided by its mean charge voltage exhibits opposite tendency. An optimized performance with energy efficiency (EE) of 80.1% was obtained when the volume ratio of water/ethanol is 7:3. In general, higher CE indicates higher selectivity, which can be characterized by vanadium permeability, whereas higher VE reveals higher conductivity which is largely determined by pore size distribution. Obviously, the efficiency change is coincident with discussed above.

Moreover, the performance of VFB assembled with membranes precipitated in 5:5 water/ethanol coagulation baths with different immersion time was investigated. As can be seen in Fig. 10, the CE decreases from 96.0% to 88.1% while VE increases from 81.1% to 88.8%, indicating declining selectivity and increasing conductivity due to enlarged pore size and wider pore size distribution. M7 exhibits the optimized performance with energy efficiency of 80.2%. The result is consistent with their area resistance date in Table 1.

Self-discharge test was also conducted to confirm the increasing degree of vanadium ions crossover with prolonged immersion time in water/ethanol coagulation bath. The test began at the state of charge of 50% and stopped when the open circuit voltage (OCV) was lower than 0.8 V. As demonstrated in Fig. 11, the OCV decay rate of the cell is in the order of M4 < M7 < M8, consisting with their columbic efficiency. For example, the self-discharge procedure of VFB cell assembled with M4 lasts for more than 70 h, which is 3 times longer than that with M8. The self-discharge results reveal the higher vanadium ions permeating rate with longer immersion time in water/ethanol coagulation bath.

In addition, single cell performance of M7 (3 min) under various current densities is shown in Fig. 12. The CE increases from 85.4% to 94.4%, which can be attributed to less vanadium ions cross-over

with higher current densities. However, VE decreases from 92.8% to 79.4%, due to increase of overpotential and ohmic resistance. The tendency is agree with previous work [8].

In the pioneered study, the chemical stability of PVDF membrane has been already proved via continuously running more than 1000 charge–discharge cycles [9]. In this paper, the capacity decay behavior was investigated via the charge–discharge cycle test at 80 mA cm^{-2} on the VFB assembled with M7. As illustrated in Fig. 13, the charge and discharge capacity declines slowly from 1.06 Ah and 0.98 Ah to 0.97 Ah and 0.92 Ah during 50 cycles, whereas the energy efficiency reminds constant at 80%, showing good battery capacity maintenance. The capacity decay is attributed to the diffusion of vanadium ions from one half-cell to the other and side reactions such as evolution of H$_2$ and oxidation of V^{2+} [29] .It is also noticeable that the overpotential increases as cycle proceeds, indicating more severe cell polarization. Moreover, no obvious change of the membrane morphology before and after running for more than 200 cycles (Fig. 14) were observed, showing good chemical stability.

4. Conclusions

In this work, PVDF membranes with different morphology were prepared via water/ethanol dual-coagulation bath. With more ethanol ratio in coagulation medium, macrovoids diminished, crystalline particles nucleated and finally fused together to form a bi-continuous structure. Such structure transition represented a crystallization-dominated phase separation ascribed to thermodynamic and kinetic hindrance. The mean pore size change leads to a non-monotonic tendency of selectivity and conductivity, thus resulting in different CE and VE. All membranes showed a

dominated β phase, even though more α phase crystals were formed in ethanol. In addition, the membrane became more porous in water/ethanol bath with prolonged time. The PVDF membrane shows good battery capacity maintenance as well as stability in VFB. Thus, the performance of PVDF membranes in VFB can be tuned via adjusting the coagulation bath.

Acknowledgments

References

[1] B. Dunn, H. Kamath, J.M. Tarascon, Science 334 (2011) 928–935.
[2] M. Skyllas-Kazacos, M.H. Chakrabarti, S.A. Hajimolana, F.S. Mjalli, M. Saleem, J. Electrochem. Soc. 158 (2011) R55.
[3] X. Li, H. Zhang, Z. Mai, H. Zhang, I. Vankelecom, Energy Environ. Sci. 4 (2011) 1147.
[4] B. Schwenzer, J. Zhang, S. Kim, L. Li, J. Liu, Z. Yang, ChemSusChem 4 (2011) 1388–1406.
[5] T. Sukkar, M. Skyllas-Kazacos, J. Appl. Electrochem. 34 (2004) 137–145.
[6] D. Xing, S. Zhang, C. Yin, C. Yan, X. Jian, Mater. Sci. Eng. B 157 (2009) 1–5.
[7] M.A. Hickner, H. Ghassemi, Y.S. Kim, B.R. Einsla, J.E. McGrath, Chem. Rev. 104 (2004).
[8] H. Zhang, H. Zhang, X. Li, Z. Mai, J. Zhang, Energy Environ. Sci. 4 (2011) 1676.
[9] W. Wei, H. Zhang, X. Li, H. Zhang, Y. Li, I. Vankelecom, Phys. Chem. Chem. Phys. 15 (2013) 1766.
[10] F. Liu, N.A. Hashim, Y. Liu, M.R.M. Abed, K. Li, J. Membr. Sci. 375 (2011) 1–27.
[11] J. Hirschinger, D. Schaefer, H.W. Spiess, Macromolecules 24 (1991) 2428–2433.
[12] A. Akbari, M. Hamadanian, V. Jabbari, A.Y. Lehi, M. Bojaran, Desalin. Water Treat. 46 (2012) 96–106.
[13] J.Y. Lai, F.C. Lin, C.C. Wang, D.M. Wang, J. Membr. Sci. 118 (1996) 49–61.
[14] M. Khayet, T. Matsuura, Ind. Eng. Chem. Res. 40 (2001) 5710–5718.
[15] M.G. Buonomenna, P. Macchi, M. Davoli, E. Drioli, Eur. Polym. J. 43 (2007) 1557–1572.
[16] X. Wang, X. Wang, L. Zhang, Q. An, H. Chen, J. Macromol. Sci. B 48 (2009) 696–709.
[17] D. Li, T.S. Chung, J. Ren, R. Wang, Ind. Eng. Chem. Res. 43 (2004) 1553–1556.
[18] Q. Luo, H. Zhang, J. Chen, D. You, C. Sun, Y. Zhang, J. Membr. Sci. 325 (2008) 553–558.
[19] Z. Mai, H. Zhang, X. Li, C. Bi, H. Dai, J. Power Sources 196 (2011) 482–487.
[20] D. Zuo, B. Zhu, J. Cao, Y. Xu, Chinese J. Polym. Sci. 24 (2006) 281–289.
[21] S.P. Deshmukh, K. Li, J. Membr. Sci. 150 (1998) 75–85.
[22] Y. Li, H. Zhang, X. Li, H. Zhang, W. Wei, J. Power Sources 233 (2013) 202–208.
[23] R. Gregorio, J. Appl. Polym. Sci. 100 (2006) 3272–3279.
[24] S. Abbrent, J. Plesti, D. Hlavata, J. Lindgren, J. Tegenfeldt, A. Wendsjo, Polymer 42 (2001) 1407–1416.
[25] P. Zapata, D. Mountz, J.C. Meredith, Macromolecules 43 (2010) 7625–7636.
[26] A.L. Ahmad, W.K.W. Ramli, W.J.N. Fernando, W.R.W. Daud, Sep. Purif. Technol. 88 (2012) 11–18.
[27] C.Y. Kuo, H.N. Lin, H.A. Tsai, D.M. Wang, J.Y. Lai, Desalination 233 (2008) 40–47.
[28] C. Sun, J. Chen, H. Zhang, X. Han, Q. Luo, J. Power Sources 195 (2009) 890–897.
[29] A. Tang, J. Bao, M. Skyllas-Kazacos, J. Power Sources 196 (2011) 10737–10747.